Pionic-decay spectra of few-body Λ hypernuclei

Izumi Kumagai-Fuse,[1] Shigeto Okabe,[2] and Yoshinori Akaishi[1]
[1]*Institute for Nuclear Study, University of Tokyo, Tanashi, Tokyo 188, Japan*
[2]*Center for Information Processing Education, Hokkaido University, Sapporo 060, Japan*
(Received 8 July 1996)

Pionic-decay spectra are discussed in $A=4$ and 5 Λ hypernuclei by using wave functions obtained by the resonating group method. For ${}^{5}_{\Lambda}$He, the π^- spectrum shows a sharp peak at 171 MeV with 1.5 MeV FWHM in the total pion energy. For ${}^{4}_{\Lambda}$H and ${}^{4}_{\Lambda}$He, the spectra have broad peaks around 170 MeV with 6–7 MeV FWHM. This difference is caused by resonance structures of the final-state nuclei under the spin-nonflip dominance in the pionic decay. Partial decay widths are calculated to check the normalization of the spectra, and are in systematically good agreement with all available experimental data. [S0556-2813(96)02612-X]

PACS number(s): 21.80.+a, 21.45.+v, 21.60.−n

I. INTRODUCTION

Weak decays of Λ hypernuclei have been measured by emulsion and bubble-chamber experiments since the discovery of a hypernucleus, where branching ratios of the decays were fairly well determined but the measured lifetimes were in large uncertainty [1–4]. Recent developments of experimental techniques have reduced the uncertainty and provided new information about partial widths of decay modes including neutral-particle emissions [5–7]. These data enable us to analyze the weak decays of Λ hypernuclei quantitatively. Thus, it is expected that the pionic weak decay provides a useful means to identify the hypernuclear species produced by counter experiments. Tamura *et al.* have obtained the production rate of ${}^{4}_{\Lambda}$H via K^- capture at rest on such light nuclei as ^{7}Li, ^{9}Be by observing weak-decay pions with discrete momentum 133 MeV/c from ${}^{4}_{\Lambda}\mathrm{H}\rightarrow{}^{4}\mathrm{He}+\pi^-$ [8]. Recently, they have also tried to extract production rates of ${}^{5}_{\Lambda}$He and ${}^{4}_{\Lambda}$He from the experimental data of the total continuum π^- spectra, which contain contributions of $A=4$ and 5 Λ-hypernuclear decays [9]. The rates are needed to reveal the production mechanism of light hyperfragments on stopped K^- reactions [10,11]. However, the pionic-decay spectra of $A=4$ Λ hypernuclei are not well determined experimentally. Therefore, detailed theoretical studies are awaited.

The purpose of this paper is to provide pionic-decay spectra of $A=4$ and 5 Λ hypernuclei. In spite of intensive studies of the decays, results obtained so far are not accurate enough to compare recent experimental data [12–16]. There are two important ingredients in order to obtain quantitative results of the spectra. One is the final-state nuclear interaction, which directly affects the spectral shape [17]. The other is the pion distortion, which considerably changes the absolute value of the spectrum [15]. Deloff has studied the decay spectra of $A=4$ hypernuclei taking into account the final-state interaction by the use of corresponding phase-shift data [14]. But he treated emitted pions with plane waves. Recently, Motoba *et al.* have taken into account the distortion effect of pions and pointed out its importance [15]. They, however, adopted simple final-state nuclear potentials, which do not well reproduce resonance behaviors of the nuclei. As a result, the fit of their pionic-decay spectrum to the data is not good in $A=5$ hypernucleus. In the present paper, we properly take into account both the ingredients to derive quantitatively the spectra, which can endure to be compared with the recent improved data.

Since nuclear resonances determine peak structures of the spectra, we describe carefully final states by using the resonating group method (RGM) which well explains low energy phenomena of $A=4$ and 5 nuclei [18,19]. This method accurately takes into account Pauli effects [20], which are substantial for pionic-decay widths. In order to check absolute magnitudes of the spectra, the pionic-decay widths are calculated by integrating the spectra and are compared with the experimental data. This investigation gives a systematical understanding of the spectra and widths, which serves as a reliable base to extract production rates of $A=4$ and 5 Λ hyperfragments from counter experiments.

This paper is organized as follows. In Sec. II we formulate the framework to calculate the pionic-decay widths and spectra by RGM. In Sec. III, calculated results are shown together with discussions. We give summary and conclusions in Sec. IV.

II. FORMULATION

Bertrand *et al.* have reported event numbers in emulsion data for each π^--decay mode of ${}^{4}_{\Lambda}$H: 914 events for the ${}^{4}\mathrm{He}+\pi^-$ decay, 301 events for the ${}^{3}\mathrm{H}+p+\pi^-$ decay, 88 events for the ${}^{3}\mathrm{He}+n+\pi^-$ decay, 12 events for the ${}^{2}\mathrm{H}+{}^{2}\mathrm{H}+\pi^-$ decay, and 5 events for four-body decays [4]. It is noted that the branching ratio of the two-body decay is about 70% of the total π^- decay in the case of ${}^{4}_{\Lambda}$H.

The hypernucleus ${}^{5}_{\Lambda}$He has no two-body decay mode, since $A=5$ nuclear systems have no bound states. The accumulated event numbers in the emulsion data are the following: 2780 events for the ${}^{4}\mathrm{He}+p+\pi^-$ decay, 15 events for the ${}^{3}\mathrm{He}+{}^{2}\mathrm{H}+\pi^-$ decay, and negligible for four-body decays [3].

By neglecting small events, we consider only the following pionic decays to two bodies and to three bodies except for the deuteron channels:

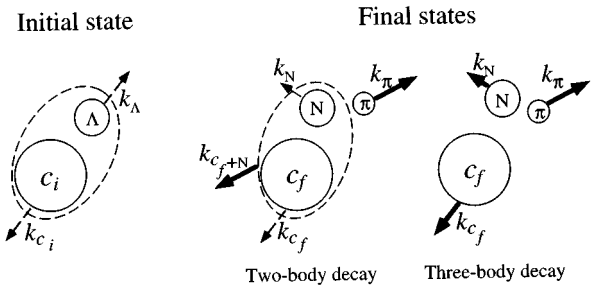

FIG. 1. Schematic picture of the pionic-decay process.

$$(c_i-\Lambda)_{\rm bound}\rightarrow(c_f-N)_{\rm bound}+\pi \tag{1}$$

$$\rightarrow c_f+N+\pi, \tag{2}$$

where c_i and c_f indicate core nuclei in the initial and the final states, respectively. A schematic picture is shown in Fig. 1. For ${}^{5}_{\Lambda}$He, the core nucleus is ^{4}He, i.e., $c_i=c_f={}^4$He. For $A=4$ hypernuclei, core nuclei are not necessarily the same between the initial and the final nuclear states. For example, $c_i={}^3$H and $c_f={}^3$He for ${}^{4}_{\Lambda}$H$({}^3\text{H}-\Lambda)\rightarrow{}^3\text{He}+n+\pi^-$, which has a sizable contribution.

The pionic-decay width Γ_{π^β} is a sum of the two-body part $\Gamma^{2b}_{\pi^\beta}$ and the three-body part $\Gamma^{3b}_{\pi^\beta}$, which are calculated by

$$\begin{pmatrix}\Gamma^{2b}_{\pi^\beta}\\ \Gamma^{3b}_{\pi^\beta}\end{pmatrix}=2\pi\int\delta(E_f-E_i)\left(\frac{L}{2\pi}\right)^3 \times d\boldsymbol{k}_{\pi^\beta}\begin{pmatrix}\left(\frac{L}{2\pi}\right)^3 d\boldsymbol{k}_{c_{f+N}}\\ \left(\frac{L}{2\pi}\right)^3 d\boldsymbol{k}_{c_f}\left(\frac{L}{2\pi}\right)^3 d\boldsymbol{k}_N\end{pmatrix}\sum_f|T^{\pi^\beta}_{fi}|^2,$$

$$E_i=M_{c_i}c^2+M_\Lambda c^2+E_{c_i\Lambda},$$

$$E_f=E_{\pi^\beta}+\begin{pmatrix}M_{c_{f+N}}c^2+\dfrac{\hbar^2k^2_{\pi^\beta}c^2}{2M_{c_{f+N}}c^2}\\ M_{c_f}c^2+M_Nc^2+\dfrac{\hbar^2k^2_{\pi^\beta}c^2}{2(M_{c_f}+M_N)c^2}+E_{c_fN}\end{pmatrix}, \tag{3}$$

where π^β denotes π^- or π^0. As shown in Fig. 1, subscripts c_f, N, and c_f+N denote a core nucleus, an emitted nucleon, and their bound system in the final state, respectively. In the case of three-body decays, $E_{c_fN}(\equiv\hbar^2k^2_{c_fN}/2\mu_{c_fN})$ in the final-state energy E_f means the relative energy of the c_f-N system. The t-matrix part $|T^{\pi^\beta}_{fi}|^2$ is given by

$$|T^{\pi^\beta}_{fi}|^2=\frac{(2\pi)^4(\hbar c)^3}{L^6E_{\pi^\beta}}\begin{pmatrix}\delta(\boldsymbol{k}_{\pi^\beta}+\boldsymbol{k}_{c_{f+N}})\\ \delta(\boldsymbol{k}_{\pi^\beta}+\boldsymbol{k}_{c_f}+\boldsymbol{k}_N)\end{pmatrix}|\widetilde{T}^{\pi^\beta}_{fi}|^2, \tag{4}$$

$$\begin{aligned}|\widetilde{T}^{\pi^\beta}_{fi}|^2&\equiv\left|\sum_{S,T}\left\langle\mathcal{A}\left[\frac{1}{\sqrt{\mathcal{N}}}[\phi_{c_f}\phi_N]_{S,T}\psi^{\rm rel}_f\right]\right|\left[s_{\pi^\beta}+ip_{\pi^\beta}\frac{(\boldsymbol{\sigma}\cdot\nabla_\pi)}{k^{(0)}_{\pi^\beta}}\right]\right.\\&\left.\times\chi^{(-)*}_{\pi^\beta}\mathcal{O}_{\Lambda\rightarrow N}\left|[\phi_{c_i}\phi_\Lambda]_S\psi^{\rm rel}_i\right\rangle\right|^2\\&=\left|\sum_{S,T}\left\langle[\phi_{c_f}\phi_N]_{S,T}\psi^{\rm rel}_f\right|\sqrt{\mathcal{N}}\left[s_{\pi^\beta}+ip_{\pi^\beta}\frac{(\boldsymbol{\sigma}\cdot\nabla_\pi)}{k^{(0)}_{\pi^\beta}}\right]\right.\\&\left.\times\chi^{(-)*}_{\pi^\beta}\left|[\phi_{c_i}\phi_N]_S\psi^{\rm rel}_i\right\rangle\right|^2,\end{aligned} \tag{5}$$

where s_{π^β} and p_{π^β} are interaction constants for the spin-nonflip and for the spin-flip processes, respectively. The π^β decay width of a free Λ particle ($\equiv\Gamma^{(0)}_{\pi^\beta}$) is proportional to $s^2_{\pi^\beta}+p^2_{\pi^\beta}$ in this framework:

$$\Gamma^{(0)}_{\pi^\beta}=\frac{2k^{(0)}_{\pi^\beta}\hbar c}{1+E^{(0)}_{\pi^\beta}/M_Nc^2}(s^2_{\pi^\beta}+p^2_{\pi^\beta}). \tag{6}$$

In order to calculate the pionic-decay widths of hypernuclei in the unit of the total-decay width of a free Λ particle, Γ_Λ, we use experimental values of the spin-nonflip–spin-flip ratio and of $\Gamma^{(0)}_{\pi^\beta}$; $s_{\pi^\beta}{}^2/(s_{\pi^\beta}{}^2+p_{\pi^\beta}{}^2)=0.88$, $\Gamma^{(0)}_{\pi^-}=0.641\Gamma_\Lambda$, and $\Gamma^{(0)}_{\pi^0}=0.357\Gamma_\Lambda$. The spin operator $\boldsymbol{\sigma}$ acts on the hyperon and the one-body operator $\mathcal{O}_{\Lambda\rightarrow N}$ converts the Λ particle into a nucleon. $k^{(0)}_{\pi^\beta}$ ($E^{(0)}_{\pi^\beta}$) is the pion wave number (total energy) which corresponds to the decay of a free Λ particle. $\chi^{(-)*}_{\pi^\beta}$ is a pion wave function, which tends to $\exp\{-i[M_{c_f}/(M_{c_f}+M_N)]\boldsymbol{k}_{\pi^\beta}\boldsymbol{r}\}$ with a relative coordinate $\boldsymbol{r}$ between $\Lambda(N)$ and a core nucleus in the plane wave limit. In the distorted wave calculation we employ an optical potential of the MSU group [21]. The modified parameter set 1 is used (see Fig. 5 in Ref. [21]) with a vertex renormalization according to the prescription by Ericson and Bando [22]. When we derive the above equations, we assume that a core nucleus of the initial state behaves as a spectator in the weak-decay process and that the conversion of the $\Lambda\rightarrow N$ occurs locally at a point since the weak interaction is regarded as of zero range.

The initial state of $A=4\Lambda$ hypernuclei with total spin $S=0$ is given by

$$|i\rangle=|[\phi_{3N}\phi_\Lambda]_{S=0}\psi^{\rm rel}_i\rangle, \tag{7}$$

where $3N$ denotes a ^{3}H or a ^{3}He cluster and $\psi^{\rm rel}_i$ is a wave function of the relative motion between Λ and $3N$. The internal wave functions are described by a harmonic oscillator shell model, where the size parameter $b_N=\sqrt{\hbar/M_N\omega}$ is taken to be 1.358 fm (1.5 fm) for ^{4}He($3N$) to fit to the rms radius. In order to derive the relative wave function, we use an effective $N\Lambda$ central interaction of YNG [23]. Since the interaction is state dependent $v^{N\Lambda}=v_0+v_\sigma(\boldsymbol{\sigma}_N\cdot\boldsymbol{\sigma}_\Lambda)+[v_r+v_{r\sigma}(\boldsymbol{\sigma}_N\cdot\boldsymbol{\sigma}_\Lambda)]P^r$, the Schrödinger equations become nonlocal. Each radial form of the interaction is written as

$$v=\sum_i w_i(k_F)e^{-(r/\beta_i)^2},$$

$$w_i(k_F)=a_i+b_i k_F+c_i {k_F}^2, \tag{8}$$

where the nuclear fermi momentum parameter k_F is taken to be 0.82 fm^{-1} and 0.90 fm^{-1} for $A=4$ and 5 Λ hypernuclei, respectively. For $A=4$ hypernuclei, the parameters are readjusted to reproduce their binding energies: For the ^1E state, w_3 is decreased by 153 (210) MeV for ${}^4_\Lambda\mathrm{H}({}^4_\Lambda\mathrm{He})$, while for the ^3E state, w_3 is increased by 153/3 (210/3) MeV.

Nuclear wave functions in the final states are determined by RGM in order to take precisely the Pauli effects into account. Coupled-channel equations of the $^3\mathrm{H}+p$ and $^3\mathrm{He}+n$ channels are solved for $\pi^-(\pi^0)$ decays of ${}^4_\Lambda\mathrm{H}({}^4_\Lambda\mathrm{He})$, while single-channel equations of isospin $T=1$ channels for $\pi^0(\pi^-)$ decays of ${}^4_\Lambda\mathrm{H}({}^4_\Lambda\mathrm{He})$. For ${}^5_\Lambda\mathrm{He}$, a $^4\mathrm{He}+N$ single-channel equation is solved. The normalized wave function $|f\rangle$ is written as

$$|f\rangle\equiv\sum_{S,T}\left|\mathcal{A}\left[\frac{1}{\sqrt{\mathcal{N}}}[\phi_{c_f}\phi_N]_{S,T}\psi_f^{\mathrm{rel}}\right]\right\rangle, \tag{9}$$

where S and T stand for spin and isospin, respectively, and $\mathcal{A}$ indicates the antisymmetrization operator between c_f and N. The internal wave function ϕ_{c_f}, which is already antisymmetrized and normalized, is described with a simple configuration of a harmonic oscillator shell model, where the size parameter is taken to be 1.46 fm. The relative wave function ψ_f^{rel} is obtained as a solution of the following equation:

$$\left(\frac{1}{\sqrt{\mathcal{N}}}\mathcal{H}\frac{1}{\sqrt{\mathcal{N}}}-E\right)|\psi_f^{\mathrm{rel}}\rangle=0. \tag{10}$$

The Hamiltonian kernel $\mathcal{H}$ and the norm kernel $\mathcal{N}$ of RGM are written as

$$\begin{pmatrix}\mathcal{H}_{STS'T'}(\boldsymbol{R},\boldsymbol{R}')\\ \mathcal{N}_{STS'T'}(\boldsymbol{R},\boldsymbol{R}')\end{pmatrix}$$
$$=\left\langle\mathcal{A}[[\phi_{c_f}\phi_N]_{S,M_S,T}\boldsymbol{R}]\left|\begin{pmatrix}\mathcal{H}_f\\ 1\end{pmatrix}\right|\mathcal{A}[[\phi_{c_f}\phi_N]_{S',M_S',T'}\boldsymbol{R}']\right\rangle. \tag{11}$$

In the present case, eigenstates of the harmonic oscillator represent eigenstates of $\mathcal{N}$. Eigenvalues of $\mathcal{N}$ have been listed in the previous paper [20]. The Hamiltonian is written as

$$\mathcal{H}_f=\sum_{i=1}^{A}t_i-T_{\mathrm{c.m.}}+\sum_{i<j}v_{ij}, \tag{12}$$

where t_i and $T_{\mathrm{c.m.}}$ are kinetic energy operators of the ith nucleon and the center-of-mass motion, respectively. We use an effective NN interaction by Nagata *et al.* [24]: NHN (and also MHN for comparison) for the central part and OPEG for the spin-orbit part. For $[^4\mathrm{He}+N]$, we multiply the strength of the spin-orbit interaction by a factor 1.35 so as to reproduce phase shifts of the $p_{3/2}$ and $p_{1/2}$ waves. It should be mentioned that the tensor part is indispensable for reproducing level structures of $A=4$ nuclei [18].

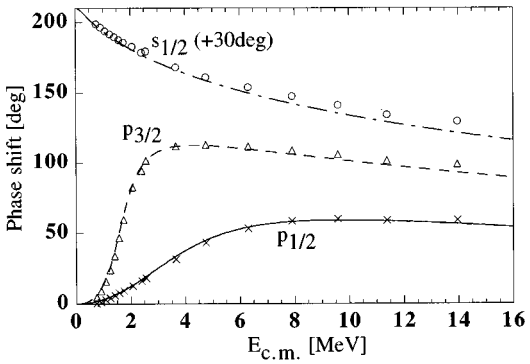

FIG. 2. The s- and p-wave phase shifts for $^4\mathrm{He}+p$. The dash-dotted line (circles), the solid line (crosses), and the dashed line (triangles) show the $s_{1/2}$, $p_{1/2}$, and $p_{3/2}$ phase shifts in the calculation (data [25]), respectively.

Calculated phase shifts of $A=4$ and 5 nuclei are compared with the experimental data [25]. In Fig. 2, we show the $^4\mathrm{He}+p$ scattering case with two resonances of $p_{3/2}$ and $p_{1/2}$. The $p_{3/2}$ resonance is the ground state of ^{5}Li, which is located around 2 MeV above the $^4\mathrm{He}+p$ threshold with 1.5 MeV width. The $p_{1/2}$ broad resonance has about 5 MeV width at 5–10 MeV above the ground state.

In ^{4}Li, phase-shift analyses have been carried out with scattering data of $^3\mathrm{He}+p$ [26]. The results show four negative-parity states with broad widths [6.03 MeV for 2^-, 7.35 MeV for 1^- (a spin-triplet main state $^3P_1$), 9.35 MeV for 0^-, and 13.51 MeV for 1^- (a spin-singlet main state $^1P_1$)]. The phase shifts of $^3\mathrm{He}+p$ are shown in Fig. 3 together with the calculated results.

We compare cases for two NN effective interactions, whose difference is in the central part. One is NHN, whose result is denoted by solid lines in the figure. The other is MHN with the vanished ^1O state part, whose result is denoted by dashed lines. This modification was done in order to reproduce the level distance of the $T=0$, 0^-, and 2^- narrow-width states in ^{4}He. The modified potential, however, is too strong for the $^1P_1$ state as seen in Fig. 3. In the pionic decay of $A=4$ hypernuclei, the $^1P_1$ state gives essential contributions to the spectra, while the $0^-,2^-$ states are not so important as discussed later. Therefore, we use the NHN potential hereafter. The calculated phase shifts of $^3\mathrm{H}+p$ and $^3\mathrm{He}+n$ are given in Fig. 4, where energies are measured from the $^3\mathrm{H}+p$ channel threshold. A cusp appears at the $^3\mathrm{He}+n$ channel threshold as seen in the $^1S_0$ phase shift of $^3\mathrm{H}+p$. The existence of the sharp $T=0$, 0^- state gives rise to a characteristic behavior of the $^3P_0$ phase shift around 2 MeV.

Thus, the resonating group method (RGM) well describes low-energy properties of $A=4$ and 5 nuclei [18,19]. This fact enables us to derive the shapes of decay spectra quantitatively as discussed in the following section.

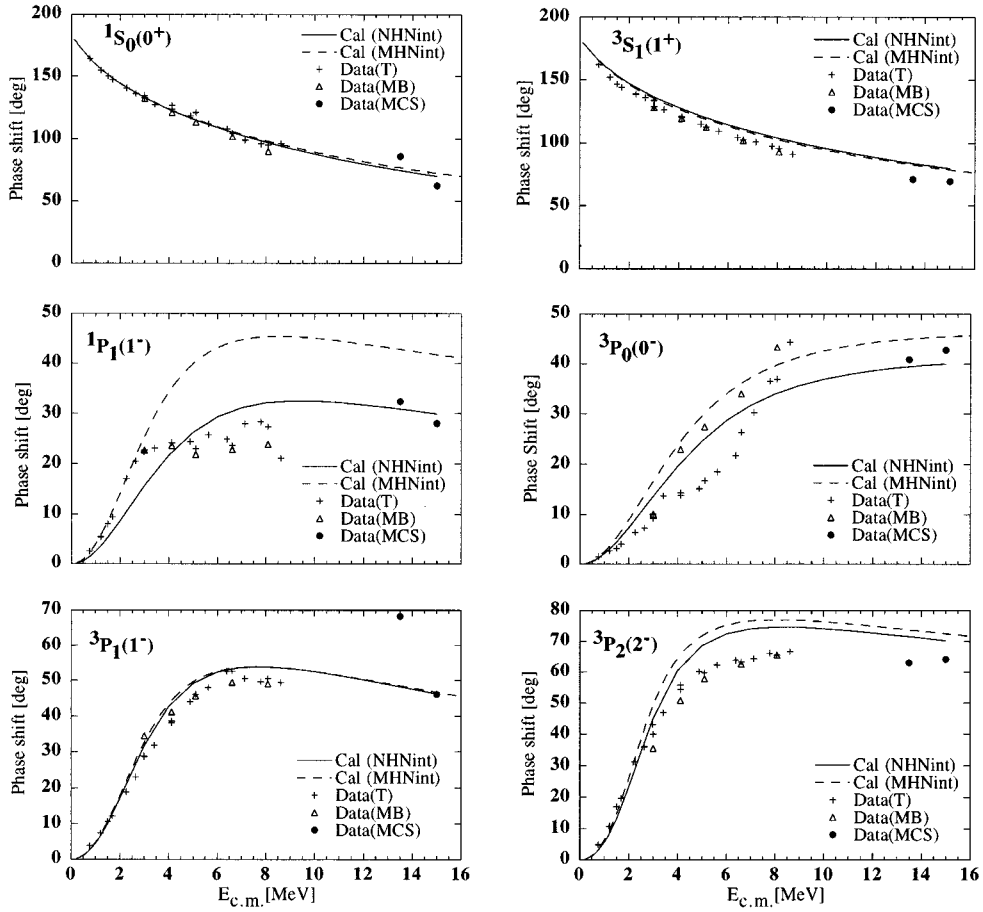

FIG. 3. The s- and p-wave phase shifts for ^{3}He+p. The solid (dashed) line shows the results calculated by the NHN (MHN with $^1O=0$) interaction set. Experimental data are denoted by pluses (by Tombrello), triangles (by McSherry *et al.*), and solid circles (by Morales *et al.*) [26].

III. RESULTS AND DISCUSSIONS

A. Pionic-decay spectra

Here we discuss the π^--decay spectra of $A=4$ and 5 Λ hypernuclei, since only π^- data are available at present. The π^0-decay spectra are theoretically expected to have similar behaviors.

The obtained π^- decay spectrum of $^5_\Lambda$He is shown in Fig. 5 together with the experimental data [3]. In the figure, we use a smearing of 0.5 MeV with Lorentzian weight, since the experimental spectrum has been obtained by counting emulsion events with an energy interval of 0.5 MeV. The calculated spectrum shows a good fit to the data.

Since the initial state of the decay is fixed to the ground state of hypernuclei, the spectra reflect the structure of the final nuclear systems. In the π^- decay of $^5_\Lambda$He, the final state is a scattering state of ^{4}He+p, which has two resonances of $p_{3/2}$ and $p_{1/2}$ as seen in Fig. 2. The two p-wave resonances determine the spectral shape: The sharp $p_{3/2}$ resonance forms a peak at the total π^- energy of about 171 MeV. The broad $p_{1/2}$ resonance changes the slope in the total π^--energy region of 160–170 MeV. The p-wave contributions to the spectrum are shown in Fig. 6 without smearing. The $p_{3/2}$ peak at 171 MeV appears in both decays through the spin-nonflip and the spin-flip terms. The $p_{1/2}$ component in the spin-flip process is negligible.

Now we discuss the π^- spectra of $A=4$ hypernuclei. The two-body pionic decay $^4_\Lambda$H$\rightarrow^4$He+π^- forms a discrete peak at 192 MeV of the total π^- energy, which corresponds to

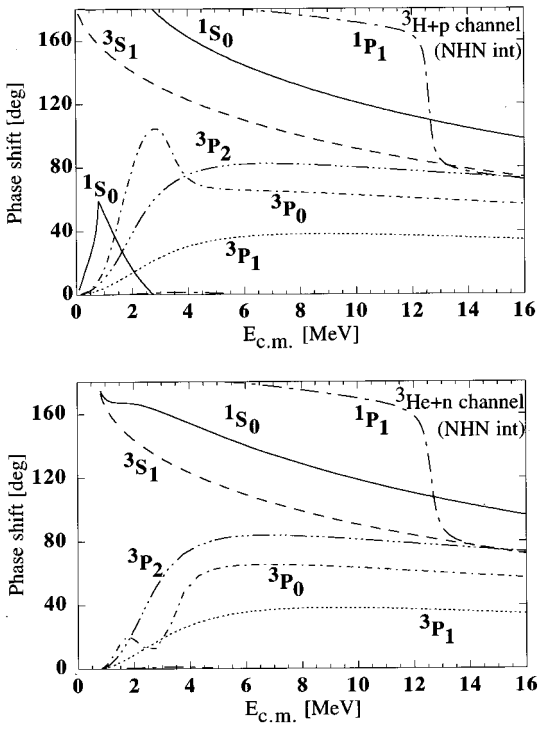

FIG. 4. The s- and p-wave phase shifts calculated by the NHN interaction set for the ^{4}He system.

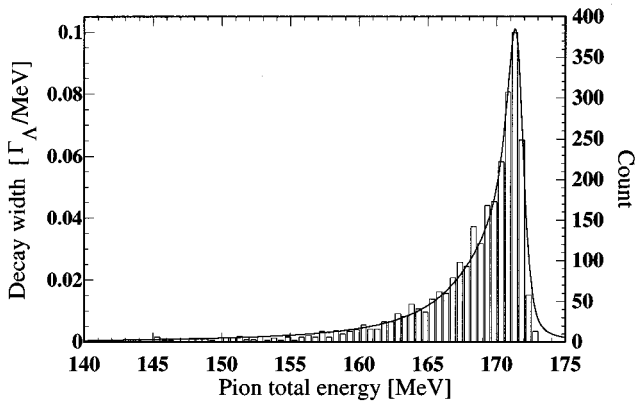

FIG. 5. The π^- energy spectrum of the ${}^{5}_{\Lambda}$He decay calculated with pion distorted waves. The histogram shows the experimental data [3].

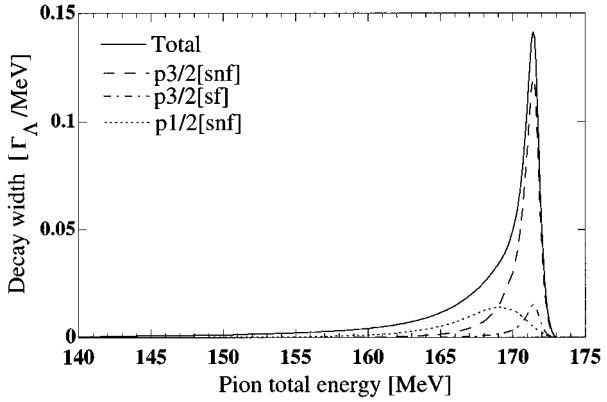

FIG. 6. The calculated π^- energy spectrum of the ${}^{5}_{\Lambda}$He decay without smearing. The solid line shows the total spectrum. The long-dashed (dash-dotted) and dotted lines denote the $p_{3/2}$ and $p_{1/2}$ components in the spin-nonflip (spin-flip) term, respectively.

133 MeV/c of π^- momentum, and its strength is given with the partial decay width, $0.618\Gamma_\Lambda$ in Table I. On the other hand, the three-body pionic decays form the continuum spectra. Similarly to ${}^{5}_{\Lambda}$He, the decay spectra reflect structures of the final-state nuclei. In ^{4}He, the lowest three isospin $T=0$ excited states have narrow widths (0.5 MeV for 0^+, 0.84 MeV for 0^-, and 2.01 MeV for 2^-). The other states have rather broad widths, and overlap each other. The obtained pionic decay spectra are shown in Fig. 7. Figures 7(a) and (b) are the spectra of the ${}^{4}_{\Lambda}\mathrm{H}\rightarrow{}^{3}\mathrm{H}+p+\pi^-$ in the spin-nonflip and spin-flip processes, respectively. The spin-nonflip term exhausts about 90% strength. Figure 7(c) is the total π^--decay spectrum of ${}^{4}_{\Lambda}$H, which is a sum of the ${}^{3}\mathrm{H}+p+\pi^-$ and the ${}^{3}\mathrm{He}+n+\pi^-$ spectra. Figure 7(d) is the total π^--decay spectrum of ${}^{4}_{\Lambda}$He. No smearing is done in the figures in order to see the intrinsic spectral shapes. The main contribution to the spectra comes from the ${}^{1}P_1$ state as seen in Figs. 7(a) and (d).

Figure 7(a) shows a sharp peak which corresponds to the $T=0,\ 0^+$ resonance state. The resonance is located between the ${}^{3}\mathrm{H}+p$ and the ${}^{3}\mathrm{He}+n$ thresholds. Then, the spectrum of ${}^{3}\mathrm{He}+n+\pi^-$ has no peak. Figure 7(b) shows a narrow peak, which comes from the $T=0,\ 0^-$, and 2^- resonances through the spin-flip term. These peaks, however, are buried in the inclusive π^- spectrum of ${}^{4}_{\Lambda}$H as shown in Fig. 7(c).

The π^- decay spectrum of ${}^{4}_{\Lambda}$He has no sharp-peak structure, as seen in Fig. 7(d), since all the ^{4}Li $T=1$ resonances have broad widths. The experimental spectrum of ${}^{4}_{\Lambda}$He is discussed in [27], though it is a crude datum that the energy interval is 1.0 MeV and the emulsion events are not so many. As seen in Fig. 8, the calculated π^- spectrum well reproduces the experimental data (Fig. 7 of [27]), where the spectrum is smeared with 1.0 MeV in view of the experimental situation.

As a summary, the π^- spectrum of ${}^{5}_{\Lambda}$He has a sharp peak with 1.5 MeV FWHM and the spectra of $A=4$ hypernuclei have broad peak structures with about 6–7 MeV FWHM, though the peak positions are almost the same around 170 MeV of the emitted-pion total energy. The difference is closely related to the final-state resonance structures in the low energy region under the spin-nonflip dominance of the pionic decay. For ${}^{5}_{\Lambda}$He, there is a sharp $p_{3/2}$ resonance in the final-state nuclear system. In addition, since the core nucleus ^{4}He is a spinless particle, the sharp resonance contributes to the spectrum independent of whether the spin of Λ changes or not. For ${}^{4}_{\Lambda}$He, there are no sharp resonances in the final-state nuclear system. For ${}^{4}_{\Lambda}$H, though low energy sharp reso-

TABLE I. Pionic-decay widths, in units of Γ_Λ, and various ratios.

${}^{4}_{\Lambda}$H	Calc.	Expt.	${}^{4}_{\Lambda}$He	Calc.	Expt.
${}^{4}\mathrm{He}\cdot\pi^-(a)$	0.618	$0.69^{+0.12}_{-0.10}$ [6]	${}^{4}\mathrm{He}\cdot\pi^0(a)$	0.348	
${}^{3}\mathrm{H}\cdot p\cdot\pi^-(b)$	0.195		${}^{3}\mathrm{He}\cdot n\cdot\pi^0(b)$	0.094	
${}^{3}\mathrm{He}\cdot n\cdot\pi^-(c)$	0.076		${}^{3}\mathrm{H}\cdot p\cdot\pi^0(c)$	0.048	
$\pi^-(d{:}a+b+c)$	0.888	$1.00^{+0.18}_{-0.15}$ [6]	$\pi^0(d{:}a+b+c)$	0.490	0.53 ± 0.07 [6]
					0.71 ± 0.10 [7]
${}^{3}\mathrm{H}\cdot n\cdot\pi^0(e)$	0.186		${}^{3}\mathrm{He}\cdot p\cdot\pi^-(e)$	0.296	0.34 ± 0.05 [6]
					0.17 ± 0.03 [7]
$\pi^0/\pi^-(e/d)$	0.210		$\pi^0/\pi^-(d/e)$	1.66	1.59 ± 0.20 [6]
					4.18(=0.71/0.17)[7]
${}^{4}\mathrm{He}\cdot\pi^-/\pi^-(a/d)$	0.695	0.69 ± 0.02 [4]	${}^{4}\mathrm{He}\cdot\pi^0/\pi^0(a/d)$	0.709	
${}^{5}_{\Lambda}$He	Calc.	Expt. [5]	${}^{5}_{\Lambda}$He	Calc.	Expt. [5]
${}^{4}\mathrm{He}+p+\pi^-$	0.386	0.44 ± 0.11	${}^{4}\mathrm{He}+n+\pi^0$	0.196	0.18 ± 0.20

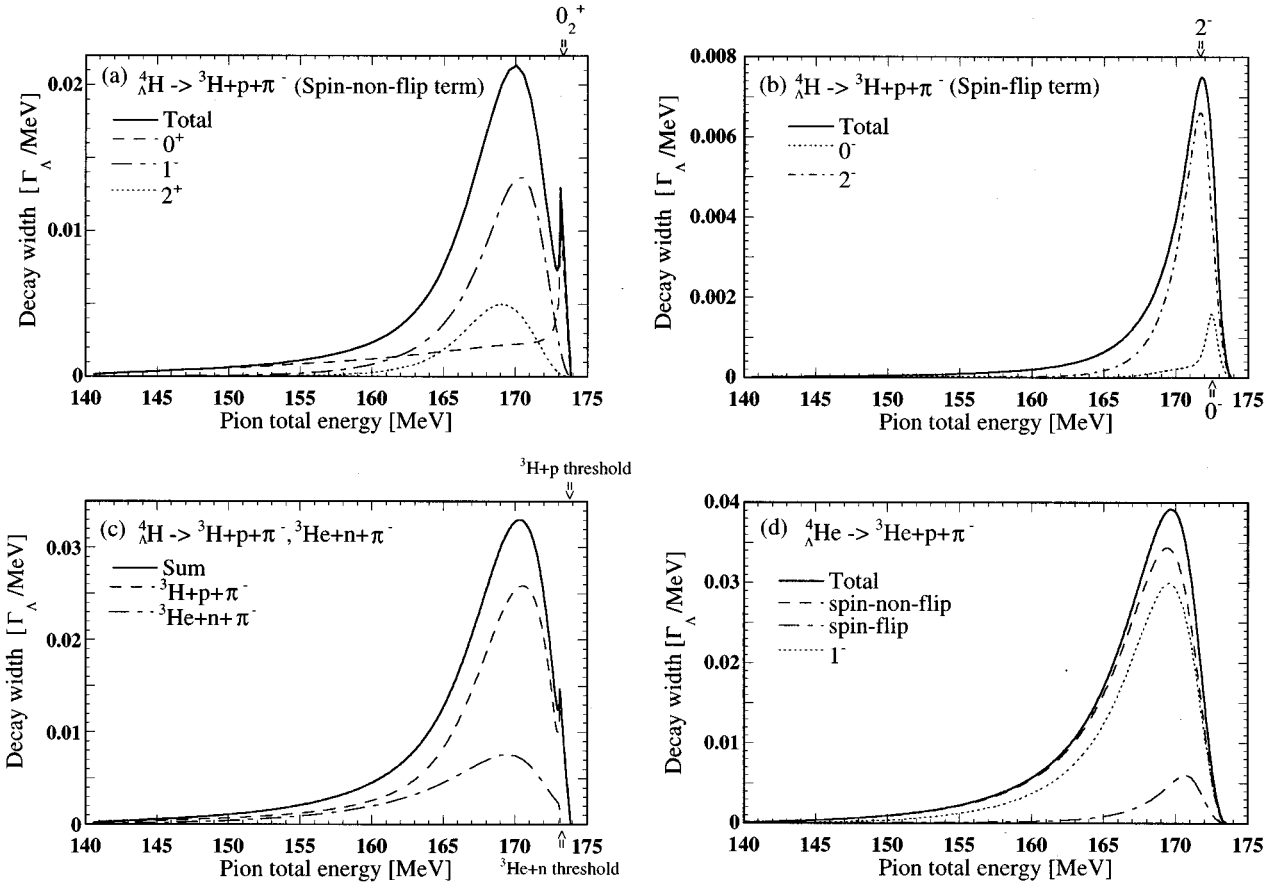

FIG. 7. (a) The calculated π^- energy spectrum for the process with the spin-nonflip term of $^4_\Lambda\mathrm{H}\rightarrow{}^3\mathrm{H}+p+\pi^-$. (b) Same as (a) with the spin-flip term. (c) The total continuum π^- spectrum of $^4_\Lambda$H. (d) The total continuum π^- spectrum of $^4_\Lambda$He.

nances exist in the final-state system, they have no large contributions to the spectrum for the following reasons: The unnatural-parity resonances cannot be excited by the spin-nonflip term, being the dominant term of the pionic decay. Though the natural-parity excited 0^+ state shows a sharp peak, its contribution is small since the s-wave decay strength is exhausted by the two-body pionic decay to the ground 0^+ state.

B. Pionic decay widths

In order to check quantitative reliability of the spectra, decay widths calculated in the same framework are compared to the recent experimental data for $A=4$ and 5 hypernuclei. They are summarized in Table I, and are in good agreement with the whole data. The values are quite similar to ones obtained in the previous paper [20], since the initial-state wave function by the YNG interaction is similar to the one solved with the Λ-nucleus potential with central repulsion.

For $^4_\Lambda$H, the two-body decay width and its ratio to the total π^--decay width are obtained to be $0.618\Gamma_\Lambda$ and 0.695, respectively, which well agree with the experimental data of $0.69(+0.12,-0.10)\Gamma_\Lambda$ [6] and 0.69 ± 0.02 [4]. The derived total π^--decay width $0.888\Gamma_\Lambda$ is also consistent with the data $1.00(+0.18,-0.15)\Gamma_\Lambda$ [6]. For $^4_\Lambda$He, there are two recent experimental data. One was measured at KEK [6], and the other was done at BNL [7]. The observed values are quite different. Our calculated results systematically support the KEK data, whose branching ratios of the π^0 and the π^- decay modes were directly measured.

The key point of the present treatment getting the overall agreement is the evaluation of Pauli suppression and enhancement effects [20] by the RGM without approximation. Since the main contributions to the pionic decays come from nuclear states below 15 MeV excitation, the Pauli principle has large effects. In the case of $^5_\Lambda$He, the π^--decay width is enhanced to $0.386\Gamma_\Lambda$ from $0.339\Gamma_\Lambda$ obtained by a simple evaluation where nonzero eigenvalues of the RGM norm are put to unity.

Since the above widths are systematically consistent with the data, the π^- spectra derived within the same framework can be reliable not only in shapes but also in absolute magnitudes.

C. Comparison with other calculations

Deloff has studied the pionic-decay spectra of $A=4$ hypernuclei carefully taking into account the final-state interaction [14]. He used angular-momentum dependent square well potentials to obtain the final-state nuclear wave functions, which reproduce the phenomenological phase-shift data of $3N+N$ systems.

The analysis of ^{4}Li* is easier than that of ^{4}He*, since low energy levels of ^{4}Li have only isospin unity due to the

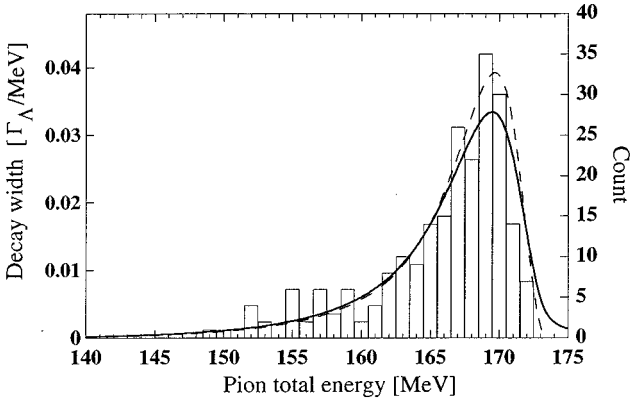

FIG. 8. The calculated π^- energy spectrum of the ${}^4_\Lambda$He decay. The dashed line is the spectra without smearing and the bold line is the one with 1.0 MeV smearing in Lorentzian weight. The histogram shows the experimental data [27].

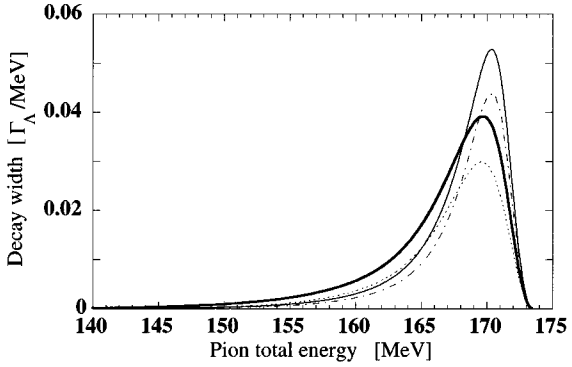

FIG. 9. The calculated π^- energy spectrum of ${}^4_\Lambda\mathrm{He}\rightarrow{}^3\mathrm{He}+p+\pi^-$. The bold (solid) line shows the total spectrum and dotted (dash-dotted) line denotes the ${}^1P_1$ component calculated with the original wave functions (${}^3P_1$ wave functions are used as the ${}^1P_1$ ones), respectively.

${}^3\mathrm{He}+p$ configuration. Even in the analysis of the ^{4}Li system, however, there remained an ambiguity for the interpretation of the two 1^- states in earlier days. Two types of solutions in the phase shift, $\delta({}^1P_1)<\delta({}^3P_1)$ and $\delta({}^1P_1)>\delta({}^3P_1)$ were proposed. Detailed discussions about this ambiguity are given in [28]. At present the former solution of $\delta({}^1P_1)<\delta({}^3P_1)$ has been accepted through analyses of spin-correlation and analyzing-power data of ${}^3\mathrm{He}+p$ scatterings [28], whose behavior agrees with that of phase shifts obtained from RGM calculations. Deloff, however, adopted the latter type of phase shifts. His ${}^1P_1$ phase shifts, which correspond to the ${}^3P_1$ ones in the present solution, are too large. The maximum phase-shift value for his potential is about 45°, while that for appropriate one is about 30° as seen in Fig. 3. Since the ${}^1P_1$ waves mainly contribute to the pionic-decay spectra of $A=4$ hypernuclei, his spectral shapes become generally sharper than the present results. To see the difference, we compare the original ${}^4_\Lambda$He spectrum with the spectrum calculated by replacing the ${}^1P_1$ wave functions with the ${}^3P_1$ wave functions of RGM (Fig. 9). The spectrum has a rather sharp peak with 4.5 MeV FWHM, while the original one has a broad peak with 6 MeV FWHM caused by the weaker ${}^1P_1$ interaction.

Recently Motoba *et al.* have also discussed the pionic-decay widths and spectra for $A=4$ and 5 hypernuclei [15]. Their partial decay widths are consistent with the present calculations except for the two-body decay widths of $A=4$ hypernuclei. In the calculation of spectra, however, they used simple Gaussian potentials to determine the final-state nuclear wave functions, which do not well-reproduce resonance behaviors of the nuclei. For example, the maximum phase-shift value for their ${}^1P_1$ potential amounts to about 60° in ^{4}Li*. Then the obtained spectra are not suitable to be used for detailed comparison with the experimental spectra.

IV. SUMMARY AND CONCLUSIONS

We have given a systematical understanding of the pionic decays of $A=4$ and 5 Λ hypernuclei by explaining consistently all the available pionic-decay data. We use RGM to determine final-state nuclear wave functions, since the microscopic cluster model has succeeded in reproducing the low-energy structures of $A=4$ and 5 nuclear systems.

Calculated π^- spectra have a peak structure around 170 MeV of the total pion energy. The peak width is largely different between $A=4$ and $A=5$ hypernuclei. For ${}^5_\Lambda$He, the spectrum has a sharp peak with 1.5 MeV FWHM. This peak is mainly formed by the $p_{3/2}$ nuclear resonance of the ^{5}Li ground state. For ${}^4_\Lambda$H and ${}^4_\Lambda$He, the spectra have broad peak structures with 6–7 MeV FWHM. These peaks are mainly formed by the ${}^1P_1$ broad resonance of $A=4$ nuclei. Though in ^{4}He sharper resonances of the $T=0$ channel exist in the low-energy region, they cannot sizably contribute to the spectrum due to their unnatural spin-parity nature.

In the present paper, we have also evaluated the partial decay widths of the hypernuclei. The calculated widths are in good agreement with the whole experimental data of $A=4$ and 5 hypernuclei. As the obtained spectrum of ${}^5_\Lambda$He shows a good fit to the data, the π^- spectra of $A=4$ hypernuclei calculated within the same framework can be regarded to be reliable. These pionic-decay spectra are necessary for the extraction of the production rates of the hypernuclei populated by means of various nuclear reactions as discussed in the Introduction.

The pionic decay is also important for identifying hypernuclei with strangeness -2 [15]. In the near future, measurements of production rates of hypernuclei would become possible not only for Λ hypernuclei but also for double-Λ ones by using pionic-decay widths and spectra. Then, such a systematical investigation of pionic-decay observables as the present work would be required for possible light double-Λ hypernuclei.

ACKNOWLEDGMENTS

The authors would like to express their gratitude to Dr. H. Outa for valuable comments and information about the experimental data. They are also thankful to the nuclear theory group of Hokkaido University for fruitful discussions.

[1] M. M. Block *et al.*, *Proceedings of the International Conference on Hyperfragment*, St. Cergue, 1963 (CERN Report 64-1), p. 63.
[2] J. P. Lagnaux *et al.*, Nucl. Phys. **60**, 97 (1964).
[3] W. Gajewski, J. Naisse, J. Sacton, P. Vilain, and G. Wilquet, Nucl. Phys. **B14**, 11 (1969).
[4] D. Bertrand, G. Coremans, C. Mayeur, J. Sacton, P. Vilain, G. Wilquet, J. H. Wickens, D. O'Sullivan, D. H. Davis, and J. E. Allen, Nucl. Phys. **B16**, 77 (1970).
[5] P. D. Barnes, Nucl. Phys. **A478**, 127c (1988); J. J. Szymanski *et al.*, Phys. Rev. C **43**, 849 (1991).
[6] H. Outa, M. Aoki, R. S. Hayano, T. Ishikawa, M. Iwasaki, A. Sakaguchi, E. Takada, H. Tamura, and T. Yamazaki, Nucl. Phys. **A585**, 109c (1995); private communication.
[7] V. J. Zeps *et al.*, in *Proceedings of the 23rd INS International Symposium on Nuclear and Particle Physics with Meson Beams in the 1 GeV/c Region*, edited by S. Sugimoto and O. Hashimoto (Universal Academy Press, Tokyo, 1995), p. 227.
[8] H. Tamura *et al.*, Phys. Rev. C **40**, R479 (1989).
[9] H. Tamura *et al.*, in *Proceedings of the 23rd INS International Symposium on Nuclear and Particle Physics with Meson Beams in the 1 GeV/c Region* [7], p. 199.
[10] T. Yamazaki, Nuovo Cimento A **103**, 78 (1989); H. Tamura, T. Yamazaki, M. Sano, Y. Yamamoto, M. Wakai, and H. Bandō, Phys. Rev. C **40**, R483 (1989).
[11] V. N. Fetisov, Nuovo Cimento A **102**, 307 (1989).
[12] R. H. Dalitz, Phys. Rev. **112**, 605 (1958).
[13] R. H. Dalitz and L. Liu, Phys. Rev. **116**, 1312 (1959).
[14] A. Deloff, Nucl. Phys. **A136**, 469 (1974).
[15] T. Motoba, H. Bandō, T. Fukuda, and J. Žofka, Nucl. Phys. **A534**, 597 (1991).
[16] U. Straub, J. Nieves, A. Faessler, and E. Oset, Nucl. Phys. **A556**, 531 (1993).
[17] I. Kumagai-Fuse and Y. Akaishi, Prog. Theor. Phys. **92**, 815 (1994).
[18] H. Furutani, H. Horiuchi, and R. Tamagaki, Prog. Theor. Phys. **62**, 981 (1979).
[19] H. Furutani, Prog. Theor. Phys. **65**, 586 (1981).
[20] I. Kumagai-Fuse, S. Okabe, and Y. Akaishi, Phys. Lett. B **345**, 386 (1995).
[21] K. Stricker, H. McManus, and J. A. Carr, Phys. Rev. C **19**, 929 (1979); J. A. Carr, H. McManus, and K. Stricker-Bauer, *ibid.* **25**, 952 (1982).
[22] M. Ericson and H. Bandō, Phys. Lett. B **237**, 169 (1990).
[23] Y. Yamamoto and H. Bandō, Prog. Theor. Phys. **73**, 905 (1985); Prog. Theor. Phys. Suppl. No. **81**, 9 (1985), Chap. II.
[24] H. Furutani, H. Kanada, T. Kaneko, S. Nagata, H. Nishioka, S. Okabe, S. Saito, T. Sakuda, and M. Seya, Prog. Theor. Phys. Suppl. No. **68**, 193 (1980), Chap. III.
[25] L. Brown, W. Haeberli, and W. Trächslin, Nucl. Phys. **A90**, 339 (1967); P. Schwandt, T. B. Clegg, and W. Haeberli, *ibid.* **A163**, 432 (1971).
[26] T. A. Tombrello, Phys. Rev. **138**, B40 (1965); D. H. McSherry and S. D. Baker, Phys. Rev. C **1**, 888 (1970); J. R. Morales, T. A. Cahill, and D. J. Shadoan, *ibid.* **11**, 1905 (1975).
[27] U. Krecker, D. Kielczewska, and T. Tymieniecka, Nucl. Phys. **A236**, 491 (1974).
[28] D. R. Tilley, H. R. Weller, and G. M. Hale, Nucl. Phys. **A541**, 1 (1992), and references therein.